Supporting Information Appendix

1. Protein sample preparation for NSE experiments

Before the NSE experiments, a phosphate buffered saline (PBS) tablet (ThermoFisher) for making 500 mL 1xPBS buffer was soaked in 2 mL D_2O (Cambridge Isotope) and vacuum dried at 80°C for 5 cycles to exchange H in the tablet into D. The deuterium exchanged PBS tablet was dissolved with 500 mL 99.9% D_2O (Cambridge Isotope) to make 1X PBS D_2O buffer. The hydrogenated $^{h}A^{h}B^{h}E$, and the selectively deuterated $^{d}A^{h}B^{d}E$, and $^{h}A^{d}B^{d}E$ complexes were exchanged into the PBS D_2O at 10.0°C, respectively, using Vivaspin 20 centrifugal concentrators of 10 kDa molecular mass cut-off. The PBS D_2O buffer exchange process was repeated for at least 5 times for each complex in order to remove residual H content in the protein solution.

Protein concentrations were determined by ultraviolet (UV) absorbance at 280 nm using a Nandrop (Thermofisher), using the extinction coefficients calculated using the ProtParam program (1) on the ExPASy Proteomics Server (us.expasy.org/). The PBS D_2O buffer was used as the background for UV absorbance measurements. The final protein concentrations used for NSE measurements were 11.2 mg/ml for $^{h}A^{h}B^{h}E$, 17.3 mg/ml for $^{h}A^{d}B^{d}E$, and 15.2 mg/ml for $^{d}A^{h}B^{d}E$. The protein solution and the PBS D_2O buffer background was loaded into a 4 mm pathlength quartz cells for NSE measurements. About 1.5 days of beamtime were needed per sample at about 1.5% sample concentration. In total, 7 days of beam time were needed to acquire the data reported in this manuscript.

2. NSE data analysis

NSE spectra and linear fittings to initial slope

The NSE I(q,t)/I(q,0) data for all the complexes were collected in q range 0.020-0.211 $Å^{-1}$. The Fourier time was from 0.5 to 477 ns in the q range 0.020-0.056 $Å^{-1}$, 0.22-194 ns in the q range 0.066-0.092 $Å^{-1}$, and 0.003 to 42 ns in q range 0.085-0.211 $Å^{-1}$.

For the hydrogenated $^{h}A^{h}B^{h}E$ complex, in the lowest q range of 0.020-0.036 $Å^{-1}$, the whole I(q,t)/I(q,0) curve fits well with a single exponential, or lnI(q,t)/I(q,0) can be fit with a linear function to obtain the decay rate $\Gamma(q)$ and $D_{eff}(q)$ according to Eq. S1. However, lnI(q,t)/I(q,0) notably deviates from linear behavior in the q range of 0.040-0.165 $Å^{-1}$ (Figure S3). Presumably, the multi-exponential decay of the I(q,t)/I(q,0) arises from the internal mode and the rotational motions of the complex. We thus obtained the initial slopes and $D_{eff}(q)$ values by linear fits of ln[I(q,t)/I(q,0)] at $t < 34.9$ ns in the q range of 0.040-0.120 $Å^{-1}$. At $t > 34.9$ ns, lnI(q,t)/I(q,0) deviates from linear function. In the q range of 0.130-0.170 $Å^{-1}$, the initial slopes and $D_{eff}(q)$ values were obtained by linear fits to lnI(q,t)/I(q,0) at $t < 10$ ns, and lnI(q,t)/I(q,0)s are distinctly nonlinear at $t > 10$ ns.

For the $^{h}A^{d}B^{d}E$ complex, in the lowest q range of 0.020-0.036 $Å^{-1}$, the entire lnI(q,t)/I(q,0) can be fit by a linear function. lnI(q,t)/I(q,0) distinctly deviates from a linear behavior in the q range of 0.040-0.211 $Å^{-1}$ (Figure S4). The initial slopes and $D_{eff}(q)$ were thus obtained by linear fits to lnI(q,t)/I(q,0) at:

t<104.2 ns in q range of 0.040-0.070 Å^{-1}
t<42.4 ns in the q range of 0.066-0.092 Å^{-1},
t<24.1 ns in the q range of 0.085-0.12 Å^{-1},
t<9.2 ns in q 0.130-0.211 Å^{-1}.

For the $^{d}A^{h}B^{d}E$ complex, in the lowest q range of 0.020-0.036 Å^{-1}, the entire lnI(q,t)/I(q,0) can be fit by a linear function. lnI(q,t)/I(q,0) distinctly deviates from linear behavior in the q range of 0.040-211 Å^{-1} (Figure S5). The initial slopes and Deff(q) were obtained by linear fits to lnI(q,t)/I(q,0) in
t<137.0 ns in the q range of 0.04-0.056 Å^{-1},
t< 42.0 ns in the q range of 0.049-0.092 Å^{-1},
t<21.1 ns in q range of 0.076-0.097 Å^{-1},
t<12.2 ns in q range of 0.085-0.120 Å^{-1},
t<6.1 ns in q range of 0.130-0.211 Å^{-1}.

NSE data analysis

The following is a summary of the theoretical analysis of NSE data. Details of the theoretical analysis are provided in references herein (35-38,45-47,66,68). Neutron spin echo spectroscopy measures the intermediate scattering function I(q,t)/I(q,0). The effective diffusion constant $D_{eff}(q)$ as a function of q is determined by the normalized intermediate scattering function I(q,t)/I(q,0):

$$\Gamma(q) = -\lim_{t\to 0}\frac{\partial}{\partial t} ln[I(q,t)/I(q,0)]$$

$$D_{eff}(q) = \frac{\Gamma(q)}{q^2} \qquad \text{Eq. S1}$$

where I(Q,0) is the static form factor. $D_{eff}(Q)$ can be calculated by the expression (2-5)**:**

$$D_{eff}(q) = \frac{k_B T}{q^2}\frac{\sum_{jl}\left\langle b_j b_l (q\cdot {H_{jl}}^T\cdot q + L_j\cdot {H_{jl}}^R\cdot L_l) e^{iq\cdot(r_j - r_l)}\right\rangle}{\sum_{jl}\left\langle b_j b_l e^{iq\cdot(r_j - r_l)}\right\rangle} \qquad \text{Eq. S2}$$

which is a generalization of the Akcasu-Gurol (AG) formula to rotational motion (5, 6). Here, b_j is the scattering length of a scattering center j, H^T is the translational mobility tensor, and H^R is the rotational mobility tensor. The coordinates r_j of the various scattering centers are taken relative to the center of *friction* of the protein, and are given by r_j (note that $\Sigma\, r_j = 0$); $k_B T$ is the usual temperature factor; and $L_j = r_j \times q$ is the torque vector for each coordinate. The brackets < > denote an orientational average over the vector q, so that

$\langle q_a q_b \exp(i\, qr)\rangle\, q^{-2} = (1/3)\delta_{ab} j_0(qr) + [(1/3)\delta_{ab} - (r_a r_b / r^2)]\, j_2(qr)$ can be expressed in terms of the spherical Bessel functions j. The translational mobility tensor H^T is defined by the velocity response $v = H^T F$ to an applied force F. The rotational mobility tensor H^R is defined by the angular velocity response $\omega = H^R \tau$ to an applied torque τ. The rotational

mobility tensor H^R can be easily determined from the translational mobility tensor H^T by inverting a 3x3 matrix (4). The scattering lengths b_j are set to 1 uniformly in the hydrogenated domains, and to 0 in deuterated domains.

The mobility tensor directly reveals internal degrees of freedom (4, 5). Given the structure of the protein, comparison of these calculations to experimental $D_{eff}(q)$ allows one to test models of the mobility tensors. For a rigid body composed of N identical subunits, the translational mobility tensor H^T is a matrix with N^2 identical 3x3 rotation elements (4) For simplicity, we take this 3x3 matrix to be the unit matrix in coordinate space, multiplied by a constant chosen to reproduce the $D_{eff}(q=0)$ for a fully hydrogenated protein complex, which must equal the diffusion constant measured by dynamic light scattering. The mobility tensor for a system with independently mobile domains does not couple these separate domains.

Comparing the calculated $D_{eff}(q)$ with data allows one to extract the relative degree of dynamic coupling between the various components of the system, for this dynamic coupling is defined by the mobility tensor**.** We calculate $D_{eff}(q)$ for the four putative models of the mobility tensor defined above in Results.

The overall diffusion constant is chosen by adjusting the diffusion constant of each scattering center to reproduce the diffusion constant of the fully hydrogenated complex. This diffusion constant is then employed separately for each of the four systems above, for the fully hydrogenated and partially deuterated complexes. This action incorporates the assumption that the diffusion constant of the partially deuterated complexes is essentially the same as the fully hydrogenated complex, in accord with our observations. We point out that the effective diffusion constant $D_{eff}(q=0)$ should be the same as the diffusion constant D_o measured by DLS *only* for the fully hydrogenated complex (7).

Calculations of $D_{eff}(q)$ of other possible models

We present data for several other models for parsing the polysyndetic ABE complex into separately mobile domains, besides the models presented in Figures 2 and 3. As a general rule, the effective diffusion constant is maximized when the separate domains are of equal size (Figure S5 Model S2A), and the effective diffusion constant becomes even larger when the complex is separated into a larger number of domains (Figure S5 Model S2B and S2C).

For completeness, we performed exhaustive calculations for the expected NSE $D_{eff}(q)$, and compared them with data, Figure S6. We find that the q-dependence of $D_{eff}(q)$ is sensitive to where we parse the ABD domain. This is particularly true for the selectively deuterated hAdBdE complex. As shown in Figure S6B, if we parse the ABD at residue 629 or at residue 639 instead of 648 (model 5, the best model), the q dependence of $D_{eff}(q)$ is different.

Figure S6C shows that in the selectively deuterated dAhBdE complex, the amplitude is quite sensitive to even a few residues difference of where we parse the N-terminal moving domain of beta-catenin: Bnterm60, 68, 81, 101 have different $D_{eff}(q)$. Thus, selective deuteration seems to make the $D_{eff}(q)$ more sensitive to the location of domain partition

for the hydrogenated component in the complex. Our model 6 remains the best explanation for the data.

To conclude the calculations, in the α-catenin homodimer, only the tip of the actin binding domain is moving separately from the complex, while the ABE complex, the entire ABD is moving.

3. Dynamic Light Scattering

To determine the center-of-mass diffusion constant D_o of the ABE, $^{h}A^{d}B^{d}E$, and $^{d}A^{h}B^{d}E$ complexes, dynamic light scattering (DLS) experiments were performed using an ALV CGS3 instrument with a fixed 90° scattering angle configuration and a 632.8 nm laser. DLS experiments were performed on the same sample used for NSE experiments, and with a series of dilutions in PBS D_2O buffer. DLS experiments were performed at 10.0±0.1 °C**.** DLS experiments suggest that ABE, $^{h}A^{d}B^{d}E$, and $^{d}A^{h}B^{d}E$ complexes have the same D_o values, Figure S6. We thus used the D_o value of $^{h}A^{h}B^{h}E$ in Figure 2.

4. Surface plasmon resonance and van 't Hoff analyses of temperature dependence of K_d

Surface-plasmon resonance (SPR) experiments were performed on a Biacore X100 instrument (GE Healthcare Life Sciences). A Biacore CM5 Biosensor chip was activated by N-hydroxysuccinimide and N-ethyl-N'-(dimethylaminopropyl) carbodiimide (GE Healthcare Life Sciences). The ligand (full-length α-catenin or EcadCT) was dissolved at 5 µg/mL in 10 mM sodium acetate, pH 4.9, and injected to coat the activated sensor chip surface in one of the two flow cells. Non-crosslinked ligand was washed away, and unoccupied sites were blocked with 1 M ethanolamine, pH 8.5. The control flow cell was activated and blocked without ligand injection.

The analytes (BE or β-catenin) were dissolved in HBS-EP buffer (10 mM HEPES, pH 7.4, 150 mM NaCl, 3 mM EDTA, 0.005% surfactant polysorbate 20) and injected in increasing concentrations over the ligand-coated surfaces at 30 µL/min for 180 seconds. The dissociation time was 800 seconds. At the end of each injection-dissociation cycle, the sensor chip was regenerated with 50 mM triethylamine, pH 9.15, 4.0 M $MgCl_2$ and HBS-EP buffer. SPR experiments were performed at from 13.0-35.0 °C for BE to α-catenin binding, and at 15.0°C for β-catenin binding to EcadCT. The Biaevaluation software provided by the instrument manufacturer was used to obtain the equilibrium dissociation constant K_d. Representative SPR sensorgrams and equilibrium binding curves are shown in Figures S7 and S8.

The enthalpy and entropy changes of the binding can be obtained from the van 't Hoff equation $RlnK_d = \frac{\Delta H}{T} - \Delta S$, where R is the gas constant, ΔH the enthalpy change, and ΔS the entropy change for the formation of the ABE complex (8): $A + BE \longrightarrow ABE$

The van 't Hoff analysis indicates an increase in entropy (positive ΔS), and a decrease in enthalpy (negative ΔH) for the formation of ABE complex, Figure S9. Although the accuracy of using van 't Hoff analysis to obtain protein-protein binding thermodynamics data has been debated (9, 10), the ΔH and ΔS obtained from our van 't Hoff analysis agrees at least qualitatively with the isothermal titration calorimetry (ITC) studies (11, 12): in particular, both the van 't Hoff analysis and the ITC studies show an entropy gain ΔS and a negative ΔH upon the formation of ABE complex, Table S2. The formation of ABE complex is thus a thermodynamically favorable process in terms of both enthalpy and entropy.

5. Calculation of conformation entropy

Quasielastic neutron scattering elastic incoherent structure factors and NMR order parameters have been used to estimate the local conformational entropy changes in proteins and in protein-ligand binding (13, 14). The contribution to conformational entropy ΔS_{conf} can be estimated from the change in phase space volume W, $\Delta S_{conf} = R\ \Delta\ \ln W$, and W can be approximated by the change in radius of gyration R_g, as the corresponding volume will scale as R_g^3:

$$\Delta S_{conf} = \Delta S_{conf,B} + \Delta S_{conf,A} = 3Rln\frac{R_{g,B\_ABE}}{R_{g,B}} + 3Rln\frac{R_{g,A\_ABE}}{R_{g,A}} \qquad \text{Eq. S3}$$

where $R_{g,A}$ and $R_{g,B}$ are R_gs of A and BE ($R_{g,B}$ is approximated as Rg_{BE} and the contribution of E is omitted because E is small as compared to B), and R_{g,A_ABE} and R_{g,B_ABE} are R_gs of α-catenin and β-catenin in the ABE complex, which have been obtained from small angle X-ray and neutron scattering (2, 15), Table S1.

6. Molecular dynamics simulation

Unbiased molecular dynamics (MD) simulation

All MD simulations were performed with the CUDA-version Amber18 (16) using the ff14SB force field (17). MD simulations were started from our recent atomic models of the ABE complex and the α-catenin dimer refined with small-angle X-ray scattering and selective deuteration/small-angle neutron scattering data (15). Both systems were solvated in a TIP3P water box (18) with 15 Å padding on each side of the box, and were neutralized by adding appropriate number of sodium and chloride ions. After minimization, the systems were heated to 300 K and equilibrated for 500 ps at constant pressure of 1 atm. Finally, two independent production simulations were carried out for 250 ns for each of the ABE complex and α-catenin dimer systems in the NPT ensemble using algorithms of Berendsen barostat (19) and Langevin thermostat (20). The Particle Mesh Ewald (PME) technique (21) with a cutoff distance of 10 Å was employed to handle the long-range electrostatic interactions, and the same threshold value was also used for the truncation of the Lennard-Jones potentials. Hydrogen atoms involved in covalent bonds were constrained by the SHAKE algorithm (22).

Root mean square deviation (RMSD) and radius of gyration (Rg) of the M and actin binding domains were calculated. RMSD converged after 150 ns, so the trajectories from 150 ns to 250 ns were used to compare the mobility of both systems. Root mean square fluctuations (RMSFs) of the α-catenin were calculated upon alignment of the M domain. Error bars were obtained by dividing the 100 ns trajectory into four 25 ns trajectories and taking the standard deviations. Principal component analysis (PCA) can transform a number of correlated variables into a smaller number of uncorrelated variables known as principal components (PCs). It is based on the analysis of a covariance (correlated atomic fluctuation) matrix obtained from an MD trajectory. Here, PCA was performed on the Cα atoms of individual residues using AmberTools (16). Only the equilibrated trajectory was used in PCA. Before the analysis, each frame was superimposed to the first frame to remove the rotational and translational degrees of freedom. The eigenvectors (PC modes) were ordered according to magnitude of the root mean-square fluctuation of the respective eigenvector.

Biased molecular dynamics (MD) simulation

Biased MD simulations, also known as steered molecular dynamics (SMD) simulations, were performed to mimic single molecule experiments in vitro. In a SMD simulation, a constant force is applied to one or more atoms, and displacement or dynamics of the system is then monitored throughout the entire simulation. An equilibrated structure of ABE taken from 150 ns of the unbiased simulations was used as the starting structure for all biased simulations. 10 pN forces with the same magnitude and opposite directions were applied on two residues – one is Ala^{698} located in H2 of ABD and the other is Arg^{684} at the N-terminus of the β-catenin Arm domain. Four independent simulations were run for 100 ns each. For comparison, we also ran four 100 ns unbiased simulations starting from the same structure as that in the biased simulations. The F-actin bound structure of ABD from Ref (23) was used as a reference structure for RMSD calculation. Since H0, part of H1 and C terminus of ABD were missing in the bound state structure, only those resolved residues were used in the calculation. Cα atoms of these residues were also used in principal components analysis (PCA).

Table S1. Rg of different components in solution and in ABE complex.

	[1]R_g (Å)
α-catenin	43.7±1.1
β-catenin	50.2±1.5
α-catenin in ABE	56.7±0.9
β-catenin in ABE	51.9±1.8

Table S2. Conformational entropy estimation of ABE complex

	[2]$T\Delta S_{conf}$ (kcal mol^{-1})	[3]$T\Delta S_{exp}$ (kcal mol^{-1})	[3]ΔH_{exp} (kcal mol^{-1})	[3]ΔG_{exp} (kcal mol^{-1})	[4]$T\Delta S_{exp}$ (kcal mol^{-1})	[4]ΔH_{exp} (kcal mol^{-1})	[4]ΔG_{exp} (kcal mol^{-1})
A+BE→ABE	0.52	5.9±1.6	-2.7±1.6	-8.6±3.2	2.2	−10.1 ± 0.1	−12.3

1. From ref. (15)
2. Estimated by Eq. S3
3. Estimated from Figure S9A and S9B using the Van't Hoff equation.
4. From ref. (12)

Supplemental Figures

Figure S1. **(A)** Complete NSE I(q,t)/I(q,0) spectra of the fully hydrogenated $^{h}A^{h}B^{h}E$ complex; **(B)-(D)** initial slope linear fitting of lnI(q,t)/I(q,0) to obtain the decay rate $\Gamma(q)$ and $D_{eff}(q)$ according to Eq. S1.

Figure S2. **(A)** Complete NSE I(q,t)/I(q,0) of the selectively deuterated $^{h}A^{d}B^{d}E$ complex; **(B)-(D)** initial slope linear fitting of lnI(q,t)/I(q,0) to obtain the decay rate $\Gamma(q)$ and $D_{eff}(q)$ according to equation S1.

Figure S3. **(A)** Complete NSE I(q,t)/I(q,0) of the selectively deuterated $^{d}A^{h}B^{d}E$ complex; **(B)-(D)** initial slope linear fitting of lnI(q,t)/I(q,0) to obtain the decay rate $\Gamma(q)$ and $D_{eff}(q)$ according to equation S1.

Figure S4. Dynamic light scattering measurements of the center-of-mass diffusion constants of **(A)** $^{h}A^{h}B^{h}E$, **(B)** $^{h}A^{d}B^{d}E$, and **(C)** $^{d}A^{h}B^{d}E$ complexes in PBS D_2O buffer. D_o used in the calculation was obtained by extrapolating the concentration dependent diffusion constants to zero concentration. Because the zero concentration D_o for all three complexes are the same, we used the D_o of the $^{h}A^{h}B^{h}E$ complex in the calculation shown in Figure 2.

Figure S5. Comparing calculations with experimental NSE $D_{eff}(q)$ data to exclude other possible models.

Figure S6. The amplitude and q-dependence of calculated $D_{eff}(q)$ are sensitive to the location to parse ABD in the linker region between M and ABD. **(A)** $^{h}A^{h}B^{h}E$ complex, **(B)** $^{h}A^{d}B^{d}E$ complex, and **(C)** $^{d}A^{h}B^{h}E$ complex. In (A)-(C), Blue and cyan dashed lines parse the moving ABD segment at residue 629 in the linker region between M and ABD. Parsing the moving beta-catenin N-terminal tail at residue 81 (cyan) raises the calculated $D_{eff}(q)$ as compared to parsing at residue 68. Magenta dashed line is a model that parsing the moving ABD at residue 639, and beta-catenin N-terminal residue 21. Red solid line is the best Model 6 shown in Figure 3 that parses the moving ABD segment at residue 648 in the linker region between M and ABD. Note that in (B) because β-catenin is deuterated, changing the location to parse the N-terminal tail of β-catenin alone does not affect $D_{eff}(q)$. However, changing the location to parse the moving ABD in the hydrogenated α-catenin has a more pronounced effect on $D_{eff}(q)$ than the fully hydrogenated complex. In (C) because α-catenin is deuterated, changing the location to parse the moving ABD does not affect the $D_{eff}(q)$. However, changing the location to parse the N-terminal tail of hydrogenated β-catenin affects the amplitude of $D_{eff}(q)$.

Figure S7. SPR sensorgrams **(A)** and binding curve; **(B)** of Beta-catenin binding to EcadCT.

Figure S8. (A) Representative SPR sensorgrams; **(B)** binding curves of BE binding to α-catenin at different temperatures.

Figure S9. (A) Temperature dependence of K_d of BE binding to alpha-catenin measured by SPR, see Figures S8 for the SPR sensorgrams**.** The multiple data points at each temperature indicate the multiple experiments performed; **(B)** van 't Hoff analysis of the K_d data to obtain free energy ΔG, enthalpy ΔH, and entropy ΔS for ABE complex formation.

Figure S10. Root mean square deviations (RMSDs) of ABE and α-catenin dimer as a function of time during the MD simulations.

Figure S11. Radius of gyration (Rg) for the M domain and ABD domains of α-catenin as a function of time during the MD simulations of the ABE complex and the α-catenin dimer.

Figure S12. Comparison of RMSFs of M domain and ABD for ABE and α-catenin dimer during the simulations (from 150 to 250 ns); the H0-H1 helices of ABD are highlighted in the box.

References Cited in Supplemental Materials

1. Gasteiger E. HC, Gattiker A., Duvaud S., Wilkins M.R., Appel R.D., Bairoch A. (2005) Protein Identification and Analysis Tools on the ExPASy Server. *The Proteomics Protocols Handbook, Humana Press (2005).* , ed Walker JM), pp 571-607.
2. Nicholl ID, *et al.* (2018) alpha-Catenin Structure and Nanoscale Dynamics in Solution and in Complex with F-Actin. *Biophys J* 115(4):642-654.
3. Callaway DJ, *et al.* (2017) Controllable Activation of Nanoscale Dynamics in a Disordered Protein Alters Binding Kinetics. *J Mol Biol* 429(7):987-998.
4. Farago B, Li J, Cornilescu G, Callaway DJ, & Bu Z (2010) Activation of nanoscale allosteric protein domain motion revealed by neutron spin echo spectroscopy. *Biophys J* 99(10):3473-3482.
5. Bu Z, Biehl R, Monkenbusch M, Richter D, & Callaway DJ (2005) Coupled protein domain motion in Taq polymerase revealed by neutron spin-echo spectroscopy. *Proc Natl Acad Sci U S A* 102(49):17646-17651.
6. Akcasu Z & Gurol H (1976) Quasi-Elastic Scattering by Dilute Polymer-Solutions. *Journal of Polymer Science Part B-Polymer Physics* 14(1):1-10.
7. Bu Z & Callaway DJ (2011) Proteins MOVE! Protein dynamics and long-range allostery in cell signaling. *Adv Protein Chem Struct Biol* 83:163-221.
8. Van Holde KE, Johnson WC, & Ho PS (2006) Principles of physical biochemistry.
9. Naghibi H, Tamura A, & Sturtevant JM (1995) Significant discrepancies between van't Hoff and calorimetric enthalpies. *Proc Natl Acad Sci U S A* 92(12):5597-5599.
10. Tellinghuisen J (2006) Van't Hoff analysis of K degrees (T): how good...or bad? *Biophys Chem* 120(2):114-120.
11. Pokutta S, Choi HJ, Ahlsen G, Hansen SD, & Weis WI (2014) Structural and thermodynamic characterization of cadherin.beta-catenin.alpha-catenin complex formation. *J Biol Chem* 289(19):13589-13601.
12. Terekhova K, *et al.* (2019) Binding partner- and force-promoted changes in alphaE-catenin conformation probed by native cysteine labeling. *Scientific reports* 9(1):15375.
13. Frederick KK, Marlow MS, Valentine KG, & Wand AJ (2007) Conformational entropy in molecular recognition by proteins. *Nature* 448(7151):325-329.
14. Fitter J (2003) A measure of conformational entropy change during thermal protein unfolding using neutron spectroscopy. *Biophys J* 84(6):3924-3930.
15. Bush M, *et al.* (2019) An ensemble of flexible conformations underlies mechanotransduction by the cadherin-catenin adhesion complex. *Proc Natl Acad Sci U S A* 116(43):21545-21555.
16. Case D, *et al.* (AMBER 2018; 2018. *University of California, San Francisco*.
17. Maier JA, *et al.* (2015) ff14SB: Improving the Accuracy of Protein Side Chain and Backbone Parameters from ff99SB. *J Chem Theory Comput* 11(8):3696-3713.
18. Jorgensen WL, Chandrasekhar J, Madura JD, Impey RW, & Klein ML (1983) Comparison of simple potential functions for simulating liquid water. *The Journal of chemical physics* 79(2):926-935.
19. Berendsen HJ, Postma Jv, van Gunsteren WF, DiNola A, & Haak JR (1984) Molecular dynamics with coupling to an external bath. *The Journal of chemical physics* 81(8):3684-3690.

20. Andersen HC (1980) Molecular dynamics simulations at constant pressure and/or temperature. *The Journal of chemical physics* 72(4):2384-2393.
21. Darden T, York D, & Pedersen L (1993) Particle mesh Ewald: An N· log (N) method for Ewald sums in large systems. *The Journal of chemical physics* 98(12):10089-10092.
22. Ryckaert J-P, Ciccotti G, & Berendsen HJ (1977) Numerical integration of the cartesian equations of motion of a system with constraints: molecular dynamics of n-alkanes. *Journal of computational physics* 23(3):327-341.
23. Xu XP, *et al.* (2020) Structural basis of αE-catenin-F-actin catch bond behavior. *eLife* 9.

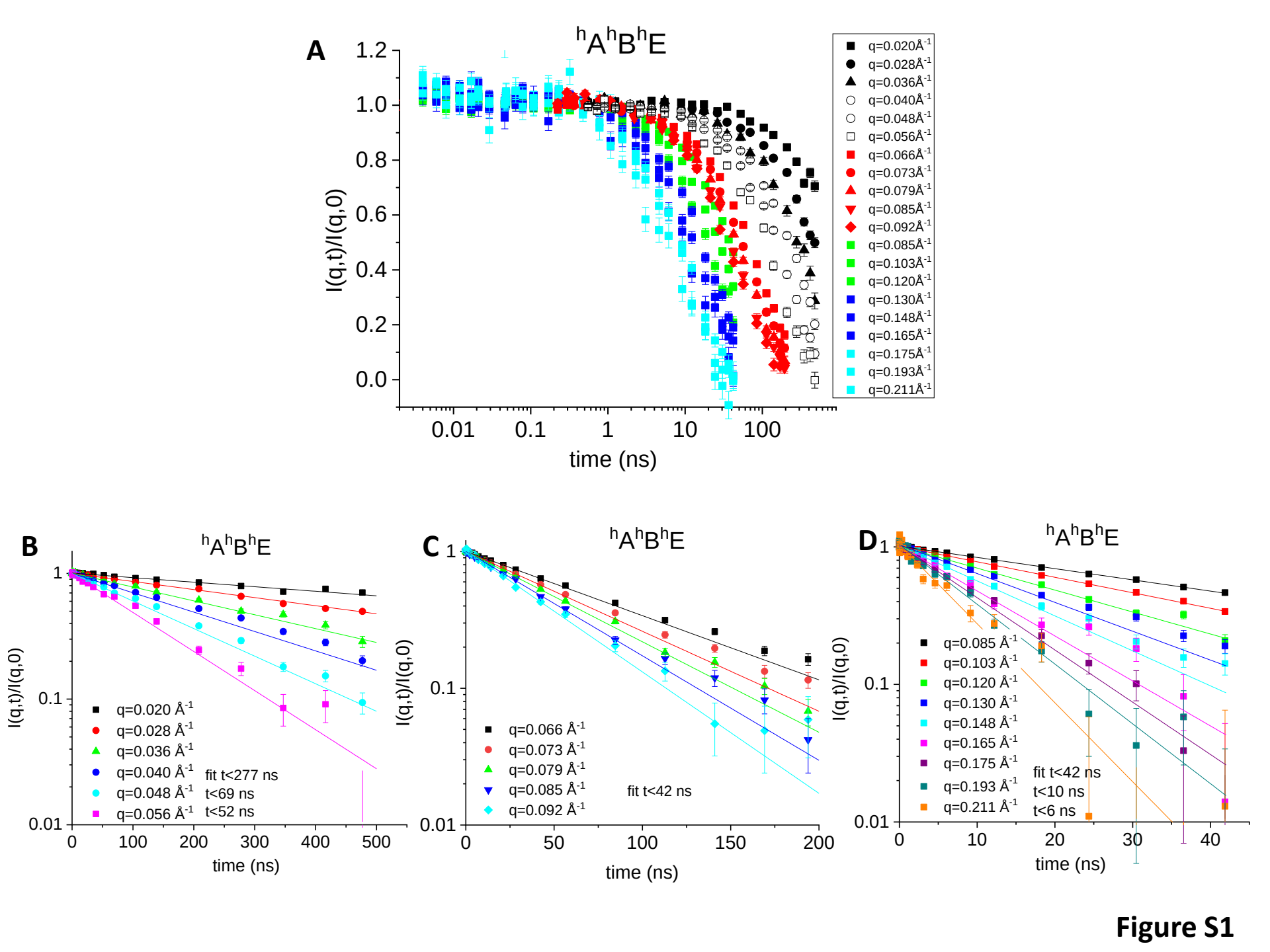
A
hAhBhE
I(q,t)/I(q,0)
time (ns)
q=0.020Å-1
q=0.028Å-1
q=0.036Å-1
q=0.040Å-1
q=0.048Å-1
q=0.056Å-1
q=0.066Å-1
q=0.073Å-1
q=0.079Å-1
q=0.085Å-1
q=0.092Å-1
q=0.085Å-1
q=0.103Å-1
q=0.120Å-1
q=0.130Å-1
q=0.148Å-1
q=0.165Å-1
q=0.175Å-1
q=0.193Å-1
q=0.211Å-1
B
hAhBhE
I(q,t)/I(q,0)
time (ns)
q=0.020 Å-1
q=0.028 Å-1
q=0.036 Å-1
q=0.040 Å-1
q=0.048 Å-1
q=0.056 Å-1
fit t<277 ns
t<69 ns
t<52 ns
C
hAhBhE
I(q,t)/I(q,0)
time (ns)
q=0.066 Å-1
q=0.073 Å-1
q=0.079 Å-1
q=0.085 Å-1
q=0.092 Å-1
fit t<42 ns
D
hAhBhE
I(q,t)/I(q,0)
time (ns)
q=0.085 Å-1
q=0.103 Å-1
q=0.120 Å-1
q=0.130 Å-1
q=0.148 Å-1
q=0.165 Å-1
q=0.175 Å-1
q=0.193 Å-1
q=0.211 Å-1
fit t<42 ns
t<10 ns
t<6 ns

Figure S1

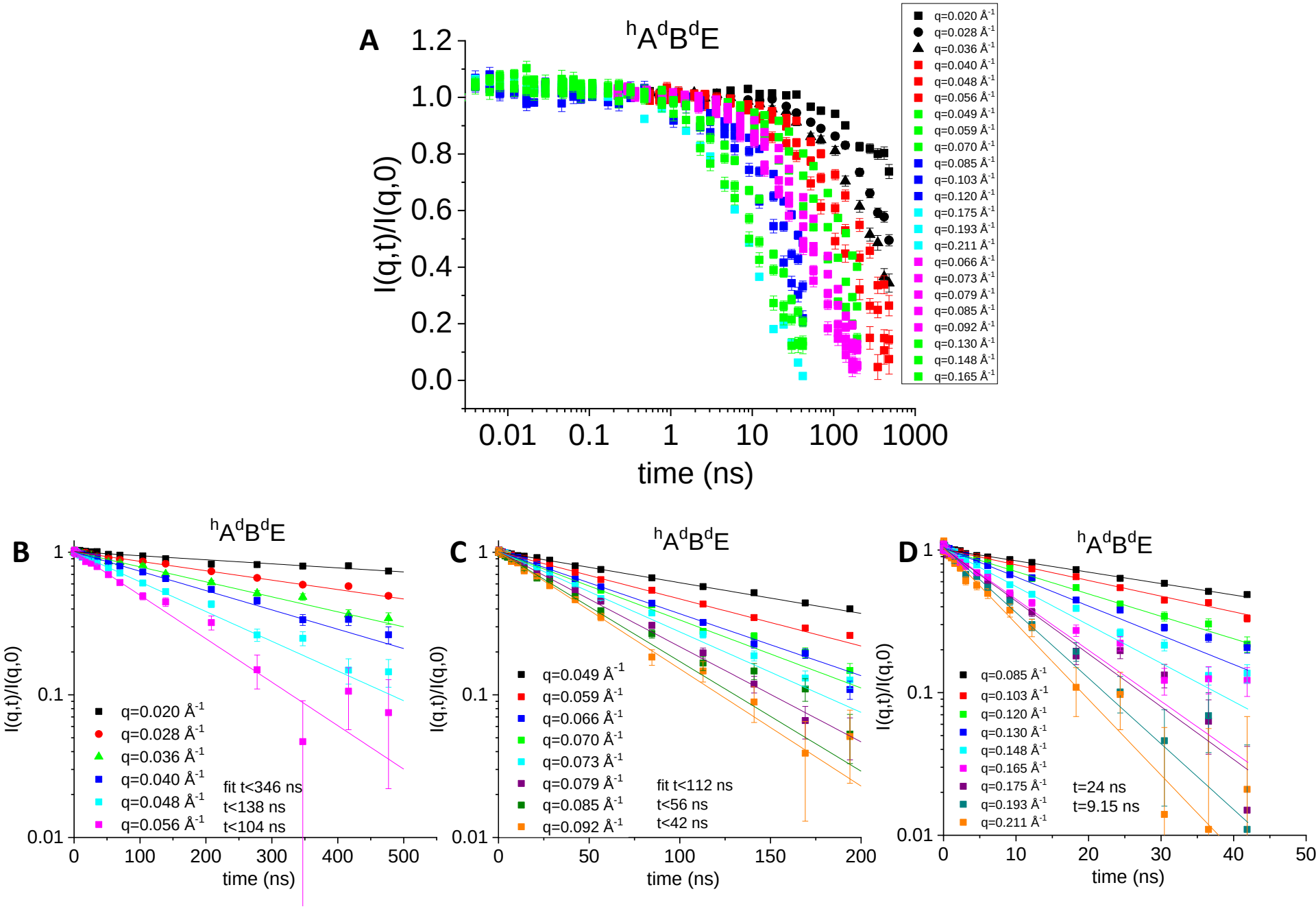
A
hAdBdE
I(q,t)/I(q,0)
time (ns)
q=0.020 Å-1
q=0.028 Å-1
q=0.036 Å-1
q=0.040 Å-1
q=0.048 Å-1
q=0.056 Å-1
q=0.049 Å-1
q=0.059 Å-1
q=0.070 Å-1
q=0.085 Å-1
q=0.103 Å-1
q=0.120 Å-1
q=0.175 Å-1
q=0.193 Å-1
q=0.211 Å-1
q=0.066 Å-1
q=0.073 Å-1
q=0.079 Å-1
q=0.085 Å-1
q=0.092 Å-1
q=0.130 Å-1
q=0.148 Å-1
q=0.165 Å-1
B
hAdBdE
I(q,t)/I(q,0)
time (ns)
fit t<346 ns
t<138 ns
t<104 ns
C
hAdBdE
I(q,t)/I(q,0)
time (ns)
fit t<112 ns
t<56 ns
t<42 ns
D
hAdBdE
I(q,t)/I(q,0)
time (ns)
t=24 ns
t=9.15 ns

Figure S2

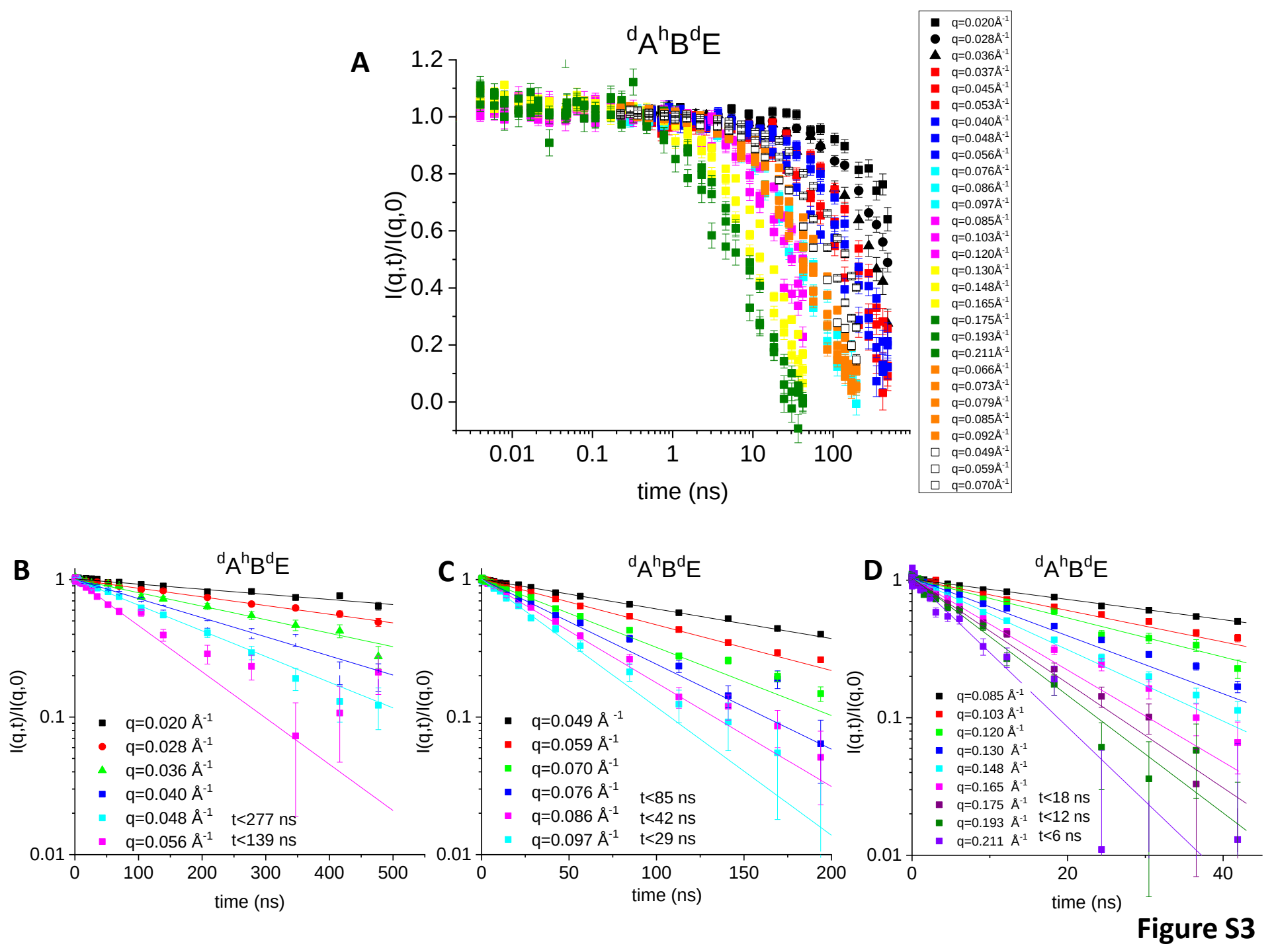
A
dAhBdE
I(q,t)/I(q,0)
time (ns)
q=0.020Å-1
q=0.028Å-1
q=0.036Å-1
q=0.037Å-1
q=0.045Å-1
q=0.053Å-1
q=0.040Å-1
q=0.048Å-1
q=0.056Å-1
q=0.076Å-1
q=0.086Å-1
q=0.097Å-1
q=0.085Å-1
q=0.103Å-1
q=0.120Å-1
q=0.130Å-1
q=0.148Å-1
q=0.165Å-1
q=0.175Å-1
q=0.193Å-1
q=0.211Å-1
q=0.066Å-1
q=0.073Å-1
q=0.079Å-1
q=0.085Å-1
q=0.092Å-1
q=0.049Å-1
q=0.059Å-1
q=0.070Å-1
B
dAhBdE
I(q,t)/I(q,0)
time (ns)
q=0.020 Å-1
q=0.028 Å-1
q=0.036 Å-1
q=0.040 Å-1
q=0.048 Å-1
q=0.056 Å-1
t<277 ns
t<139 ns
C
dAhBdE
I(q,t)/I(q,0)
time (ns)
q=0.049 Å -1
q=0.059 Å-1
q=0.070 Å-1
q=0.076 Å-1
q=0.086 Å-1
q=0.097 Å-1
t<85 ns
t<42 ns
t<29 ns
D
dAhBdE
I(q,t)/I(q,0)
time (ns)
q=0.085 Å-1
q=0.103 Å-1
q=0.120 Å-1
q=0.130 Å-1
q=0.148 Å-1
q=0.165 Å-1
q=0.175 Å-1
q=0.193 Å-1
q=0.211 Å-1
t<18 ns
t<12 ns
t<6 ns

Figure S3

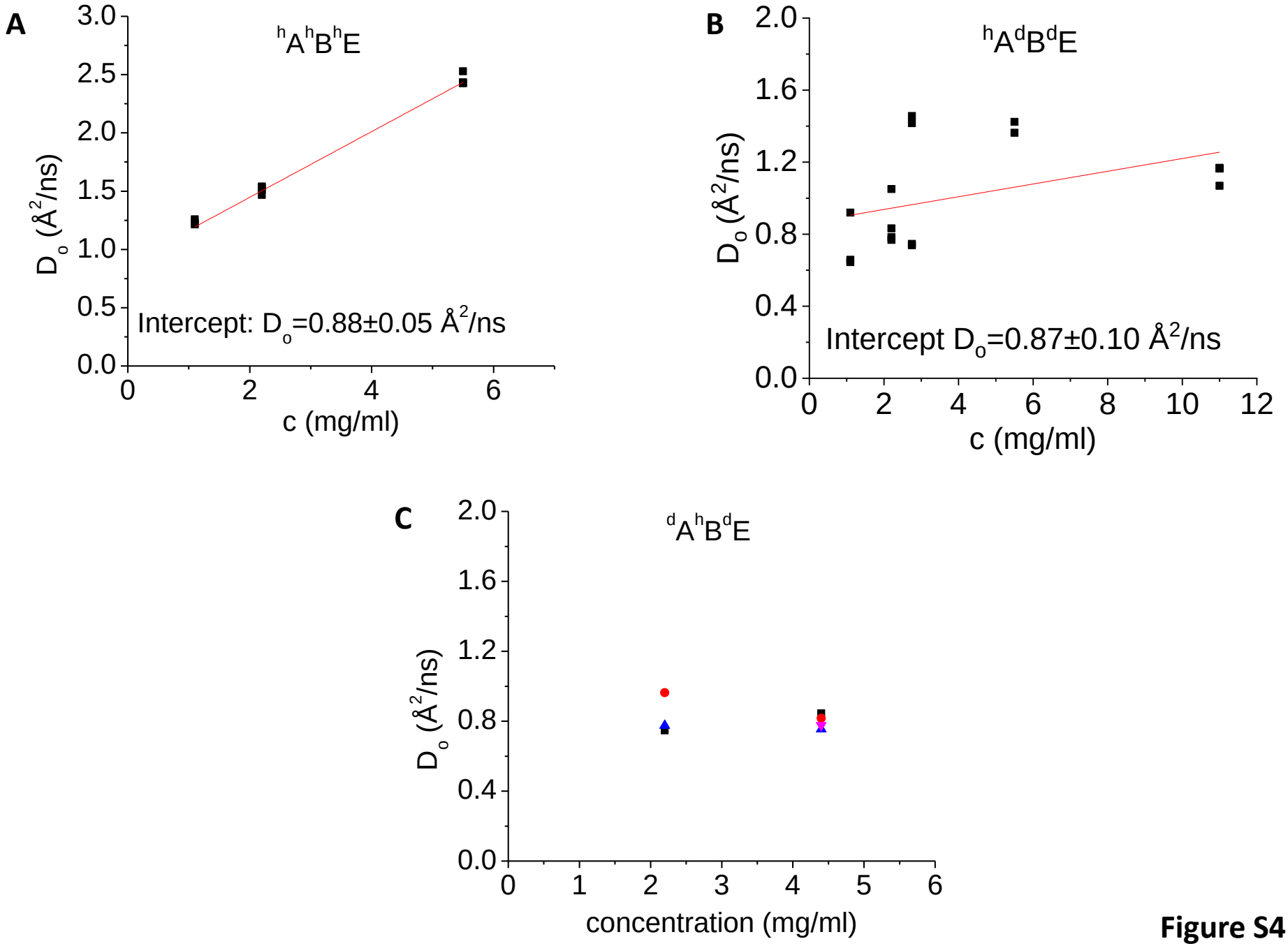
A
$^{h}A^{h}B^{h}E$
D_o (Å^2/ns)
Intercept: D_o=0.88±0.05 Å^2/ns
c (mg/ml)
B
$^{h}A^{d}B^{d}E$
D_o (Å^2/ns)
Intercept D_o=0.87±0.10 Å^2/ns
c (mg/ml)
C
$^{d}A^{h}B^{d}E$
D_o (Å^2/ns)
concentration (mg/ml)

Figure S4

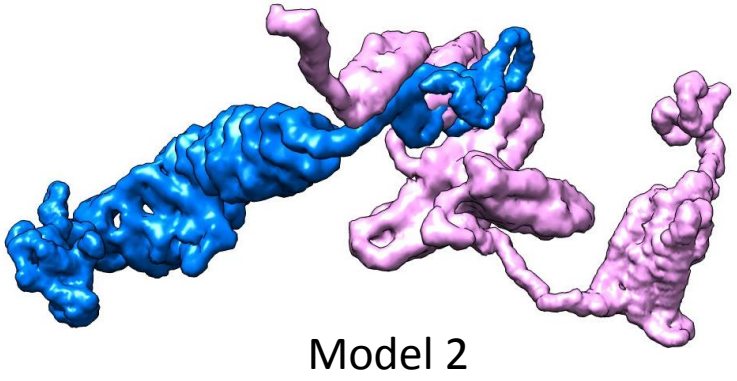

Model 2

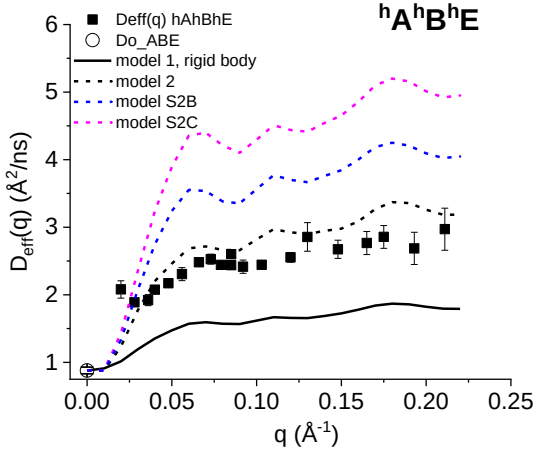

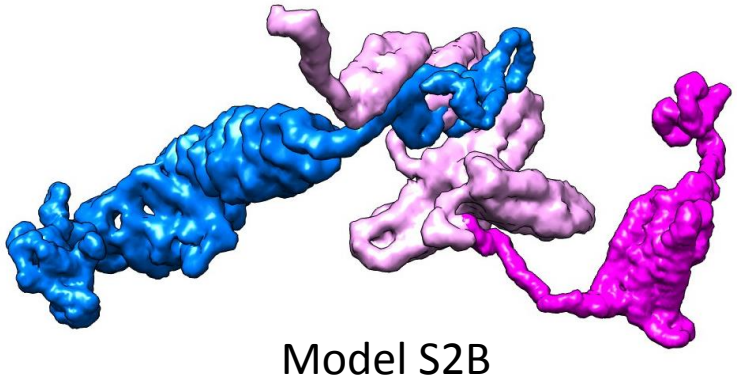

Model S2B

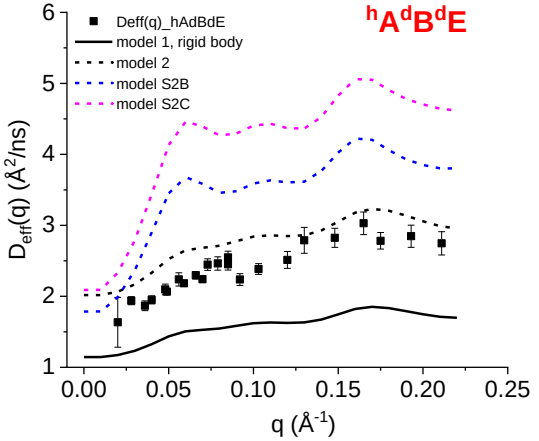

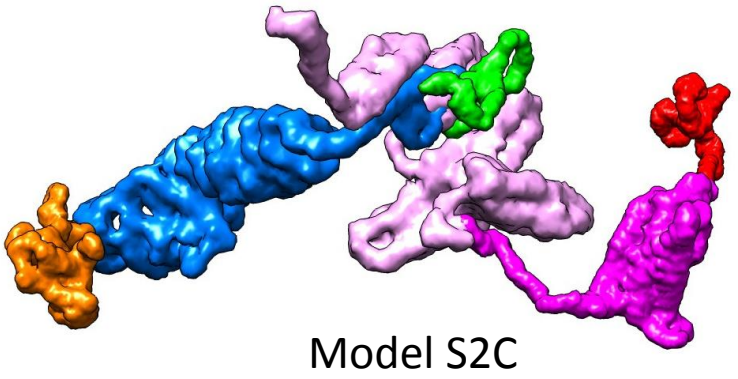

Model S2C

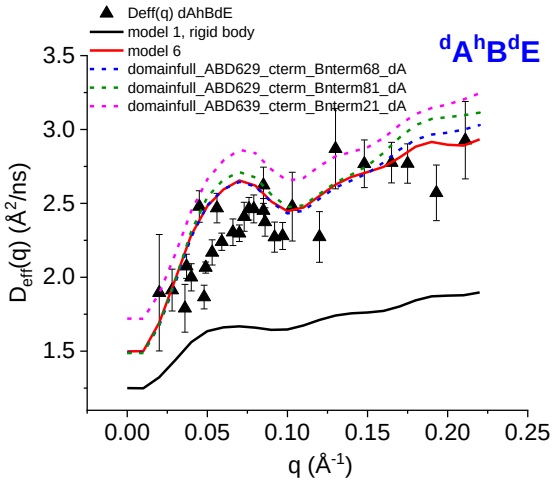

Figure S5

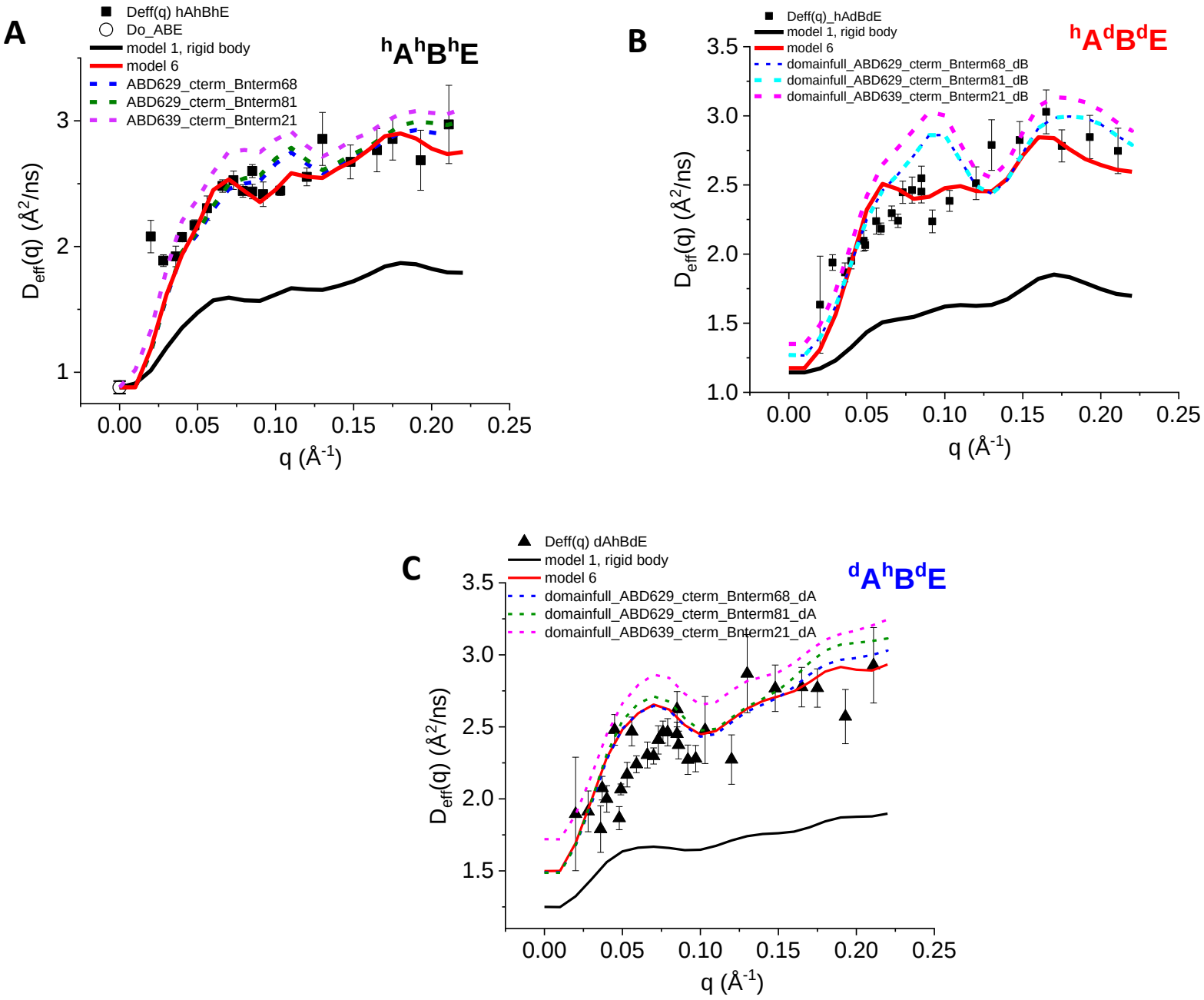
A
Deff(q) hAhBhE
Do_ABE
model 1, rigid body
model 6
ABD629_cterm_Bnterm68
ABD629_cterm_Bnterm81
ABD639_cterm_Bnterm21
hAhBhE
Deff(q) (Å2/ns)
q (Å-1)
B
Deff(q)_hAdBdE
model 1, rigid body
model 6
domainfull_ABD629_cterm_Bnterm68_dB
domainfull_ABD629_cterm_Bnterm81_dB
domainfull_ABD639_cterm_Bnterm21_dB
hAdBdE
Deff(q) (Å2/ns)
q (Å-1)
C
Deff(q) dAhBdE
model 1, rigid body
model 6
domainfull_ABD629_cterm_Bnterm68_dA
domainfull_ABD629_cterm_Bnterm81_dA
domainfull_ABD639_cterm_Bnterm21_dA
dAhBdE
Deff(q) (Å2/ns)
q (Å-1)

Figure S6

A

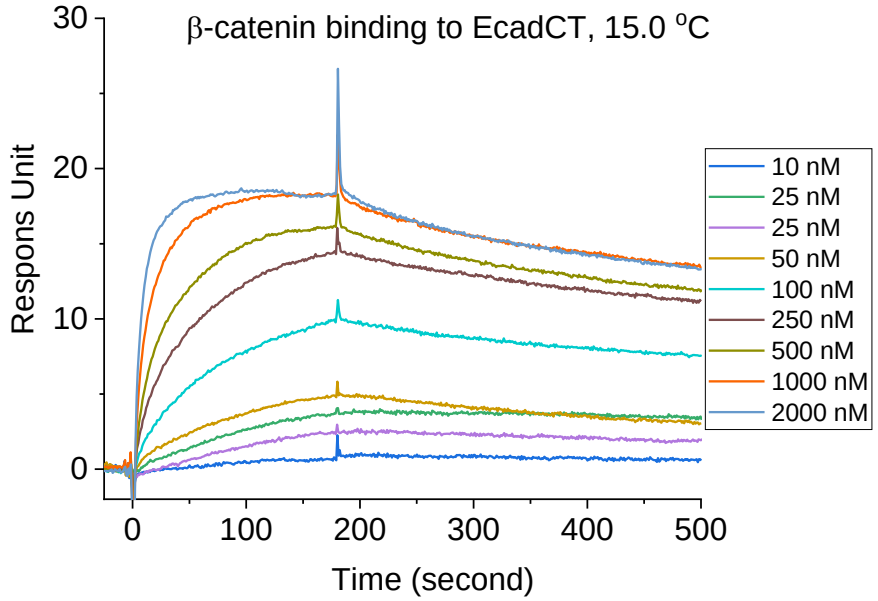
β-catenin binding to EcadCT, 15.0 °C
Respons Unit
Time (second)
10 nM
25 nM
25 nM
50 nM
100 nM
250 nM
500 nM
1000 nM
2000 nM

B

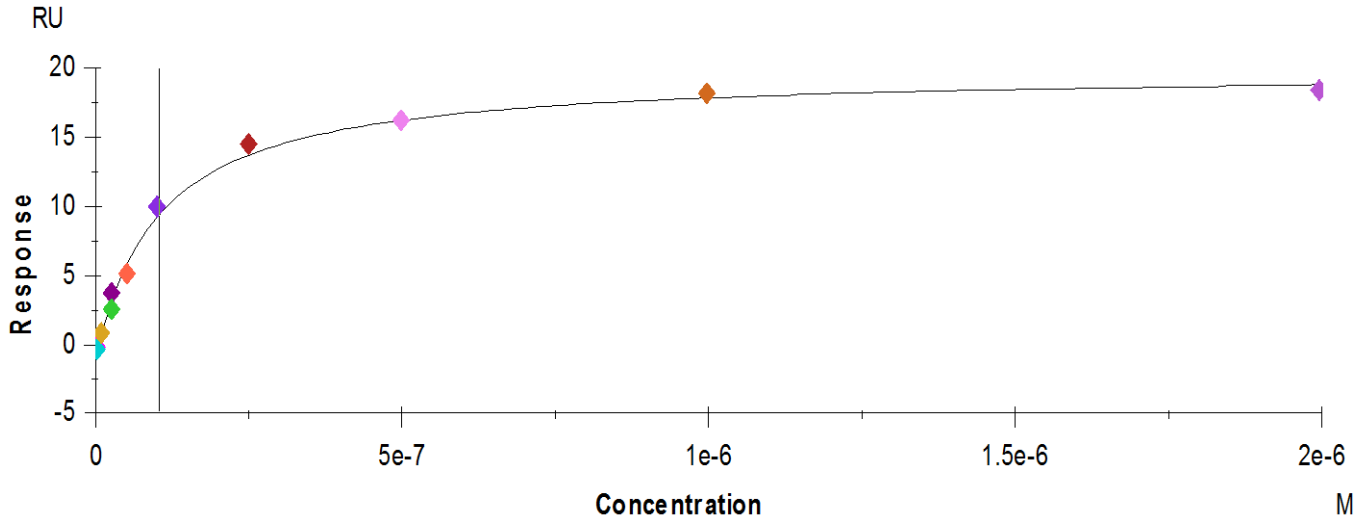
RU
Response
Concentration
M

Figure S7

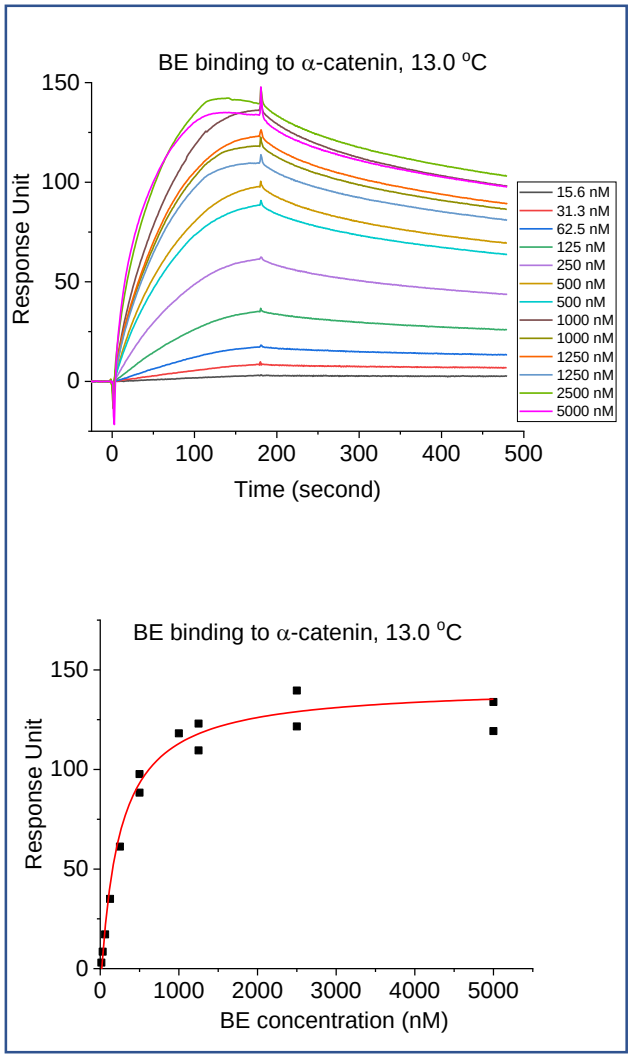
BE binding to α-catenin, 13.0 °C
Response Unit
Time (second)
15.6 nM
31.3 nM
62.5 nM
125 nM
250 nM
500 nM
500 nM
1000 nM
1000 nM
1250 nM
1250 nM
2500 nM
5000 nM
BE binding to α-catenin, 13.0 °C
Response Unit
BE concentration (nM)

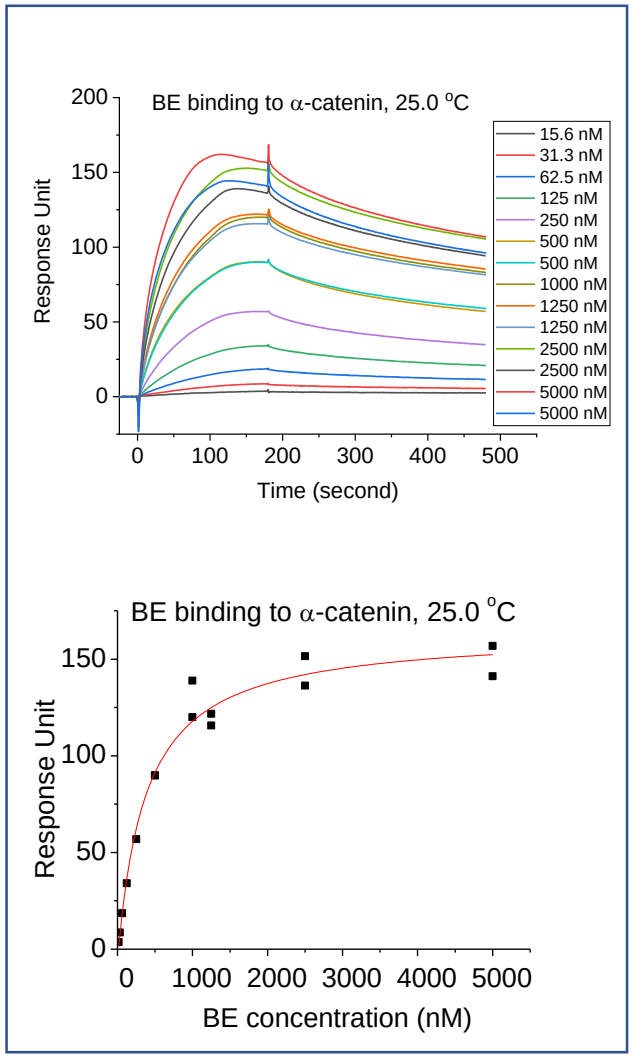
BE binding to α-catenin, 25.0 °C
Response Unit
Time (second)
15.6 nM
31.3 nM
62.5 nM
125 nM
250 nM
500 nM
500 nM
1000 nM
1250 nM
1250 nM
2500 nM
2500 nM
5000 nM
5000 nM
BE binding to α-catenin, 25.0 °C
Response Unit
BE concentration (nM)

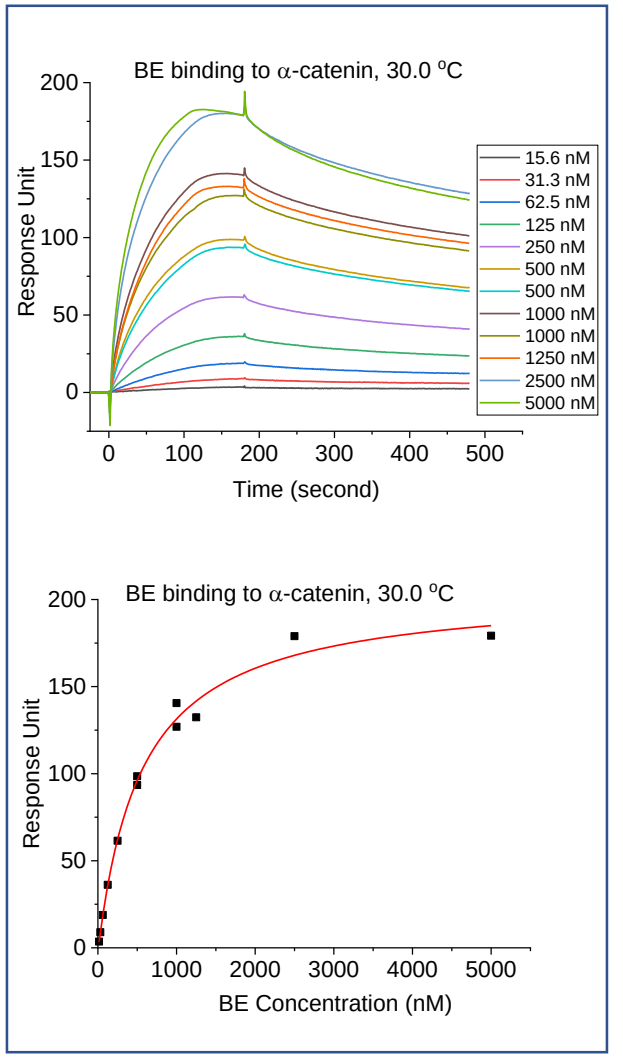
BE binding to α-catenin, 30.0 °C
Response Unit
Time (second)
15.6 nM
31.3 nM
62.5 nM
125 nM
250 nM
500 nM
500 nM
1000 nM
1000 nM
1250 nM
2500 nM
5000 nM
BE binding to α-catenin, 30.0 °C
Response Unit
BE Concentration (nM)

Figure S8

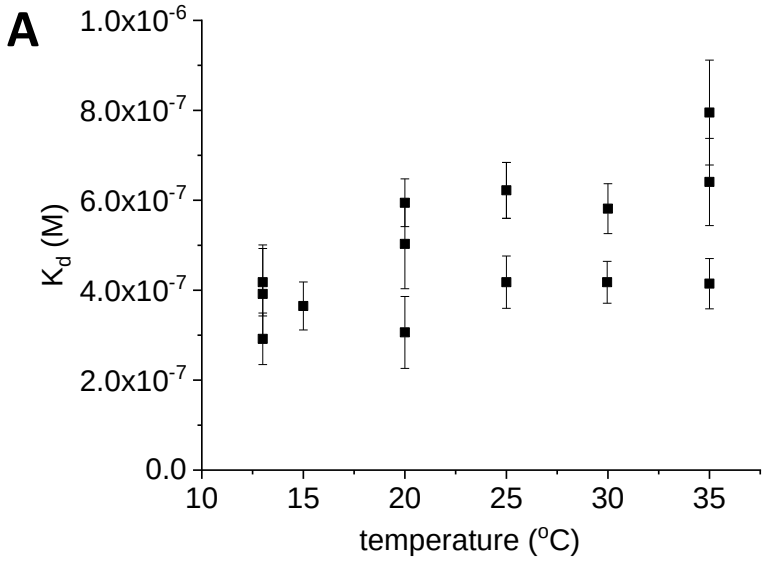
A
1.0x10-6
8.0x10-7
6.0x10-7
4.0x10-7
2.0x10-7
0.0
Kd (M)
10
15
20
25
30
35
temperature (oC)

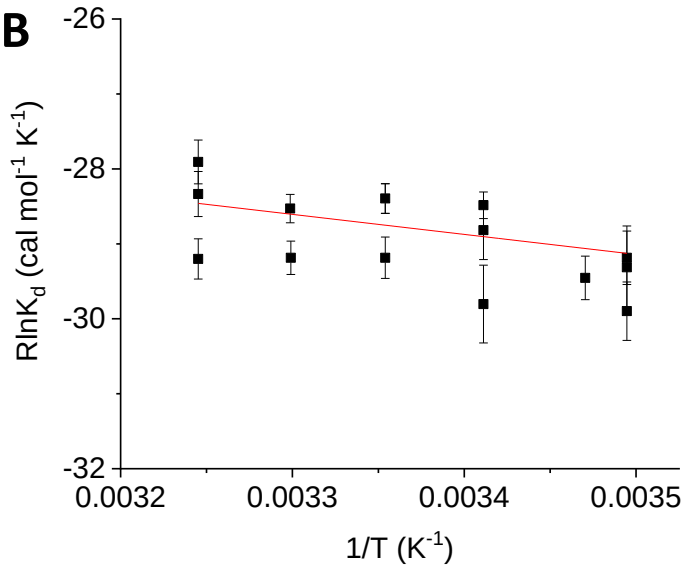
B
-26
-28
-30
-32
RlnKd (cal mol-1 K-1)
0.0032
0.0033
0.0034
0.0035
1/T (K-1)

Figure S9

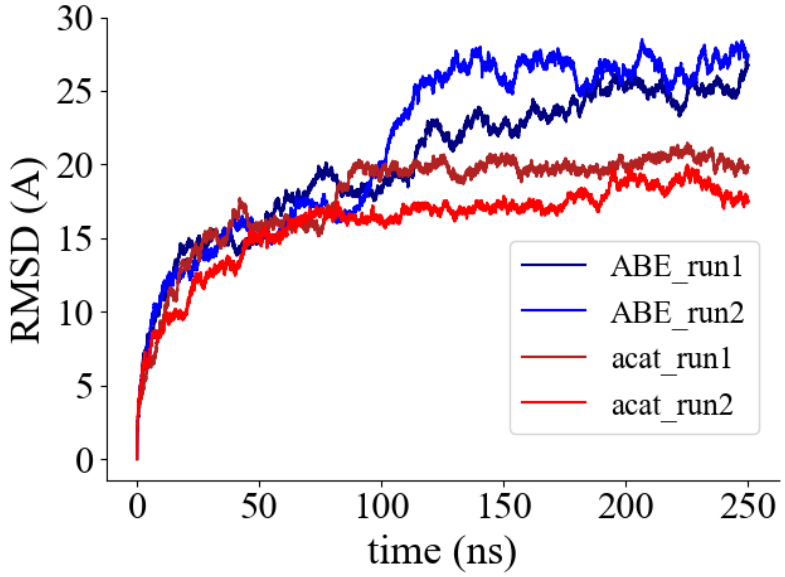
RMSD (A)
time (ns)
0
5
10
15
20
25
30
0
50
100
150
200
250
ABE_run1
ABE_run2
acat_run1
acat_run2

Figure S10

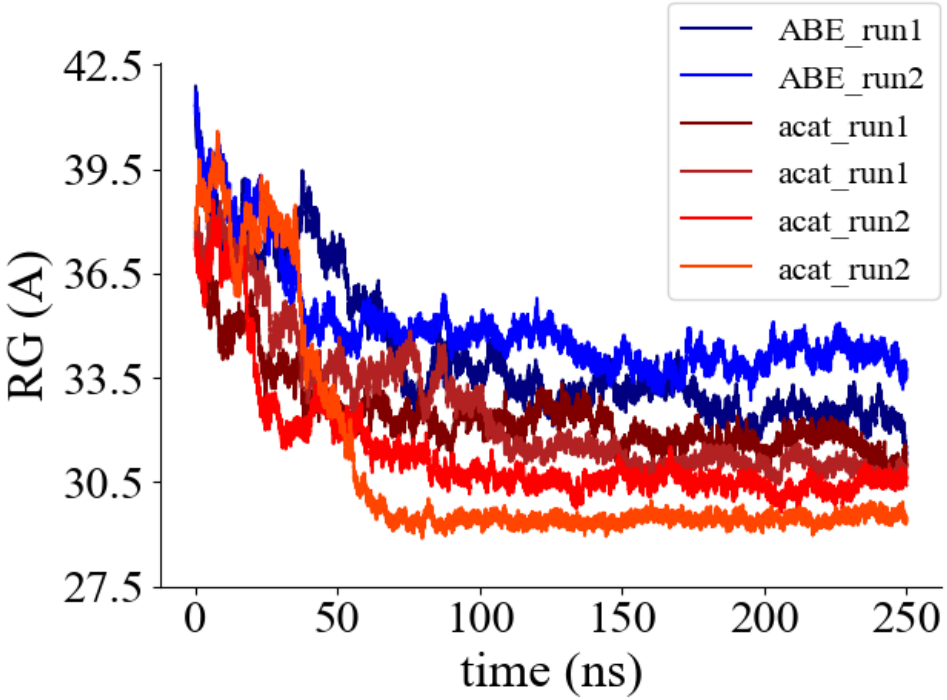
ABE_run1
ABE_run2
acat_run1
acat_run1
acat_run2
acat_run2
42.5
39.5
36.5
33.5
30.5
27.5
RG (A)
0
50
100
150
200
250
time (ns)

Figure S11

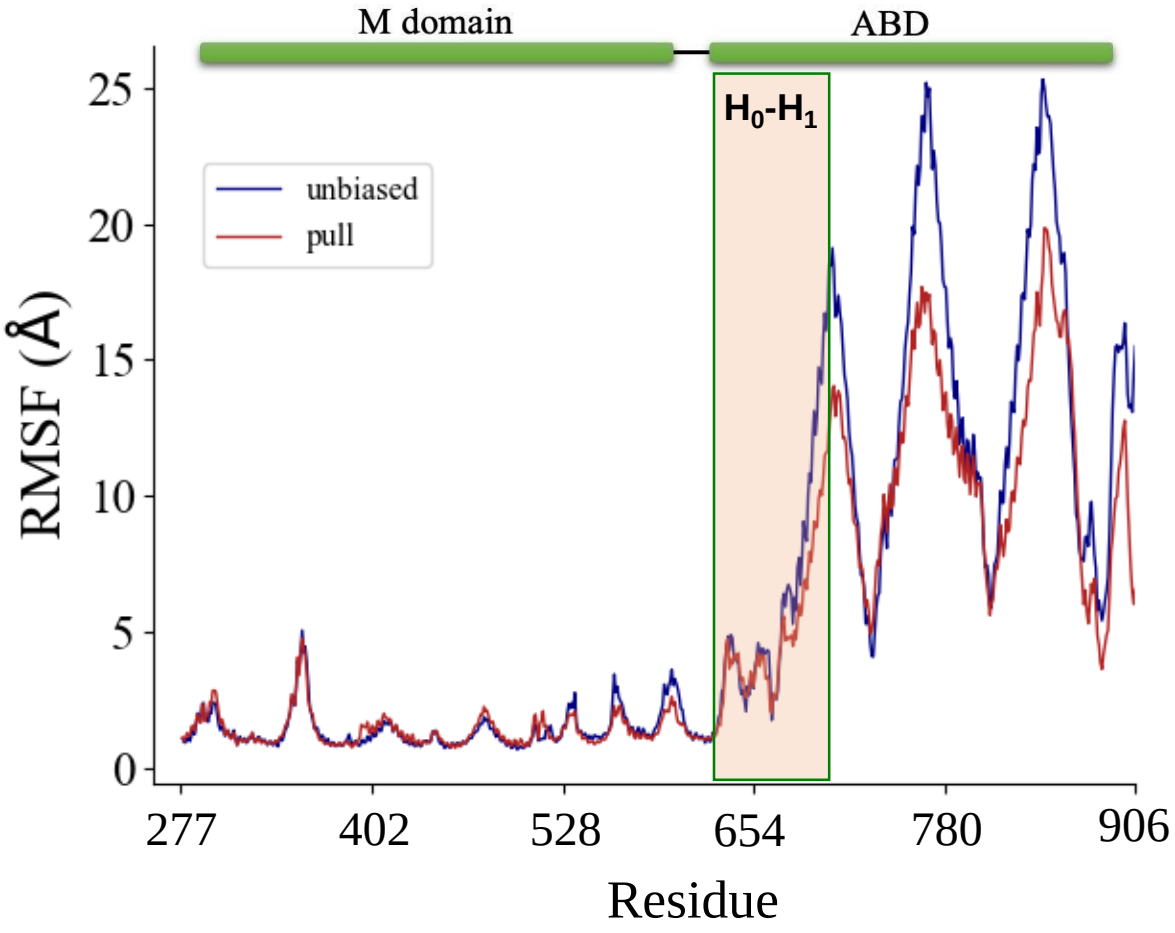
M domain
ABD
H0-H1
unbiased
pull
RMSF (Å)
25
20
15
10
5
0
277
402
528
654
780
906
Residue

Figure S12